Local Structure Studies of As-Made Cu_{2}ZnSnS_{4} Nanoparticles

Leila Jewell, Sophia Rocco, Frank Bridges, and Sue A. Carter

Local Structure Studies of As-Made Cu_2ZnSnS_4 Nanoparticles

Leila Jewell,[1] Sophia Rocco,[1] Frank Bridges,[1, *] and Sue A. Carter[1]

[1]*Physics Department, University of California, Santa Cruz, California 95064, USA*

(Dated: May 12, 2017)

Though Cu_2ZnSnS_4 (CZTS) is a promising material for thin film solar cells, a significant challenge remains in understanding the structures being formed, particularly in non-stoichiometric materials. We use the extended x-ray absorption fine structure (EXAFS) technique to study the local structure and stoichiometry of as-made, Cu-deficient, CZTS nanoparticles and present K edge data and fits about each of the cations (Cu, Zn, Sn). The data show that all the metal-S (M-S) pairs have the bond lengths of the kesterite structure within 0.02 Å, and the pair distribution function is very narrow ($\sigma \sim 0.07$ Å). This precludes significant fractions of other phases with different M-S bondlengths. The data also reveal some Sn second neighbors about Sn whereas there are none in the stoichiometric kesterite (or stannite) structure. Consequently, Sn antisite defects must be present on Cu or Zn sites; this is not surprising since there is some excess of Sn. More importantly, the second neighbor Sn-Sn distance is significantly longer than other M-M distances and the antisite Sn defects must therefore introduce significant disorder within the Cu and Zn sub-lattices. The largest distortions are found about Cu and are modeled using a strongly broadened (or split) peak distribution for the Cu-Cu/Zn pairs. We also find that excess Zn does not go onto Cu sites but rather onto Sn sites. The samples are best described as a kesterite structure with significant antisite disorder.

I. INTRODUCTION

Cu_2ZnSnS_4 (CZTS) has many desirable properties for solar cell applications: low-cost, abundant materials, an optimal bandgap, and promising initial solar energy conversion efficiencies.[1] Some of the highest efficiency devices have been fabricated from solution-processible nanoparticles[2] as the starting material rather than bulk materials. The nanoparticles may form different structure and/or stoichiometry than bulk systems.

Controlling the stoichiometry and structure of CZTS in general has proved challenging.[3,4] The materials ZnS and Cu_2S are nearly immiscible[5] and SnS_2 is needed to stabilize the CZTS structure. Because the range of stability in the ZnS-Cu_2S-SnS_2 phase diagram is small,[6] many samples made at low temperatures are not stoichiometric. The stoichiometry of nanoparticles can be tuned to have a band gap of 1.5 eV, which has applications in photovoltaics and LED lighting.[7,8]

A major difficulty, however, is in characterizing the local structures that form within CZTS and related materials, about each of the cations. The local arrangement of atoms is very similar to the cubic zinc-blende structure such as cubic ZnS, with four S nearest neighbors and twelve metal second neighbors. The ordering of the metal atoms leads to the kesterite or stannite structure, with the primary difference arising from an interchange of the Zn and and one of the Cu atom sites between the two structures.[9]

The environments about each cation are consequently very similar, as seen in the crystal structure, shown in Fig. 1. In diffraction, the main Bragg peaks of CZTS are at nearly the same position as that of several related compounds and components, including Cu_2SnS_3 and ZnS, which makes it very difficult to distinguish such

components. Additionally, the grain size in thin films can be small, leading to broader peaks, and for small nanoparticles, often only a few broad diffraction peaks remain. Other groups have synthesized CZTS materials in powder[10], thin film[11], and some EXAFS studies have been carried out on these materials;[12–17] XANES studies at the S edge (and at the Se K edge for CZTSe) have also been carried out for thin film samples[18,19] but there is little to compare directly with our data. However we include these results in the Discussion section.

Here we study the local structure in as-made, slightly off-stoichiometry nanoparticles of CZTS, to see how or if the structure differs from bulk materials. Here the samples are Cu-poor, as Guo *et al.*[2] note that such materials makes better devices, while other phases form for Cu-rich samples. We use the extended x-ray absorption fine structure (EXAFS) technique, to determine the environment around Cu, Zn, and Sn, out to the third shell of neighbors. Some earlier EXAFS studies[12–14,16] have investigated local structure in CZTS materials, but many are not in nanoparticle form; also they have rather different results, which will be compared in the Discussion. In addition we use the absorption step-height for each metal element to estimate atomic ratios and hence the composition. This approach provides a direct measure of the stoichiometry of the sample under study, and the composition extracted from step heights agrees well with other methods such as EDX[20] and atomic absorption[21].

Espinosa-Faller et al.[16] study the local structure of stoichiometric CZTS in nanoparticle form. Our two (different) nanoparticle samples are both slightly copper poor, which may produce better devices[1,2,4,22]. Due to the Cu deficiencies, the two samples are also either zinc rich or tin rich, which provides some contrast. It is important to see if these shifts in the stoichiometry
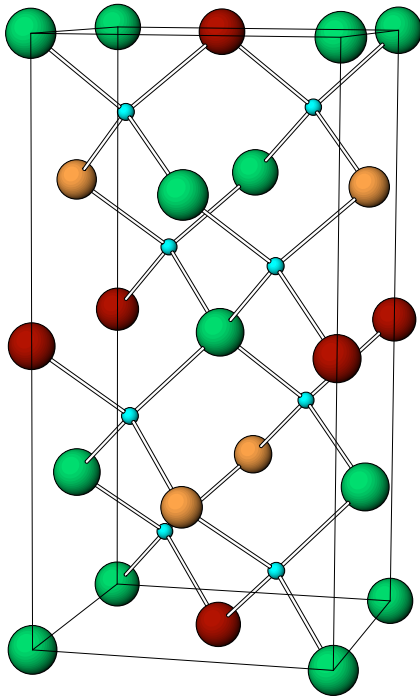
FIG. 1: The structure of kesterite Cu_2ZnSnS_4; the unit cell is tetragonal (space group $I\bar{4}$). The Cu atoms are green spheres, the Zn atoms are orange spheres, the Sn atoms are dark red spheres, and the S atoms are small light blue spheres. Other possible structures are stannite CZTS and zinc-blende CZTS. Stannite is nearly identical to kesterite, only the Zn sites switch locations with one of the two Cu sites. This change is indistinguishable to EXAFS since Cu/Zn are neighbors in the periodic table. A third possible CZTS structure is a distorted zinc-blende structure, which has a random distribution of metal atoms on the cation sites.

change the local structure of CZTS, such as whether significant clustering occurs or whether the cations have the approximate orderings required for the known Kesterite and Stannite structures. Additionally, because Cu_2SnS_3 and ZnS have very similar diffraction patterns, one needs to determine if phase separation occurs; i.e. whether significant fractions of these two (or other) compounds are also present. A complication for nanoparticle samples is that the diffraction peaks become significantly broadened and the difference between CZTS, Cu_2SnS_3, ZnS and other similar phases cannot be resolved. Unfortunately, because Cu and Zn are neighbors in the periodic table, the EXAFS signals for Cu and Zn are nearly identical and one cannot distinguish between Cu and Zn neighbors.

II. EXPERIMENTAL DETAILS

A. Samples

For this study, two different nanoparticle materials ($\sim$ 7 nm) were purchased from Mesolight which were prepared in June of 2014.[2,23] We have diffraction data for these samples but only three broad peaks are observed at the positions of the three dominant lines, and that is not useful for understanding the structure. For the EXAFS samples, the nanoparticles, suspended in toluene, were deposited onto filter paper by pipetting the solution onto the paper and then evaporating the solvent. Using multiple cycles of pipetting and evaporation, sufficient CZTS was deposited into the filter paper so that with several layers of filter paper to adjust the step height for each edge, the x-ray absorption could be measured in transmission.

B. Data Collection

The EXAFS data were collected at the Stanford Synchrotron Radiation Lightsource (SSRL) on beamlines 11-2 and 4-1 (unfocused mode) using a Si (220) double monochromator, detuned 30% for all edges to reduce harmonics. Slit heights were approximately 0.5 mm, which gives energy resolutions of $\sim$ 0.9 eV for Cu and Zn and $\sim$6.9 eV for Sn. The Cu, Zn, and Sn K edge data were collected in transmission mode at a temperature of 50 K for Sample # 1 and 8 K for Sample #2. A minimum of three scans were collected for each edge for averaging and to check reproducibility. Previous studies of bulk ZnS have shown very little change in the EXAFS data from 8 to 50 K[24,25], with no change in the first (Zn-S) peak and only a tiny change of a few percent in the second peak (Zn-Zn), thus there is no significant temperature effect.

In addition, XANES data were collected at the same time for each edge. In each case the data for the two samples overlapped very well. The only clear change is a tiny (1%) increase in the pre-edge peak near 8985 eV for the Cu K edge XANES of sample #1, which has a larger Cu/Zn ratio, compared to sample #2. In contrast the recent work of Colina-Ruiz et al.[17] find that this peak decreases slightly for larger Cu/Zn ratiosi (but for larger Cu/Sn ratios). Thus tiny changes in the Cu pre-edge peak do not provide a clear monitor of composition and we do not consider the XANES further.

III. DATA

A. EXAFS data

The EXAFS data were reduced using standard procedures,[26] which include removing the pre-edge background using the Victoreen equations[27] for transmis-
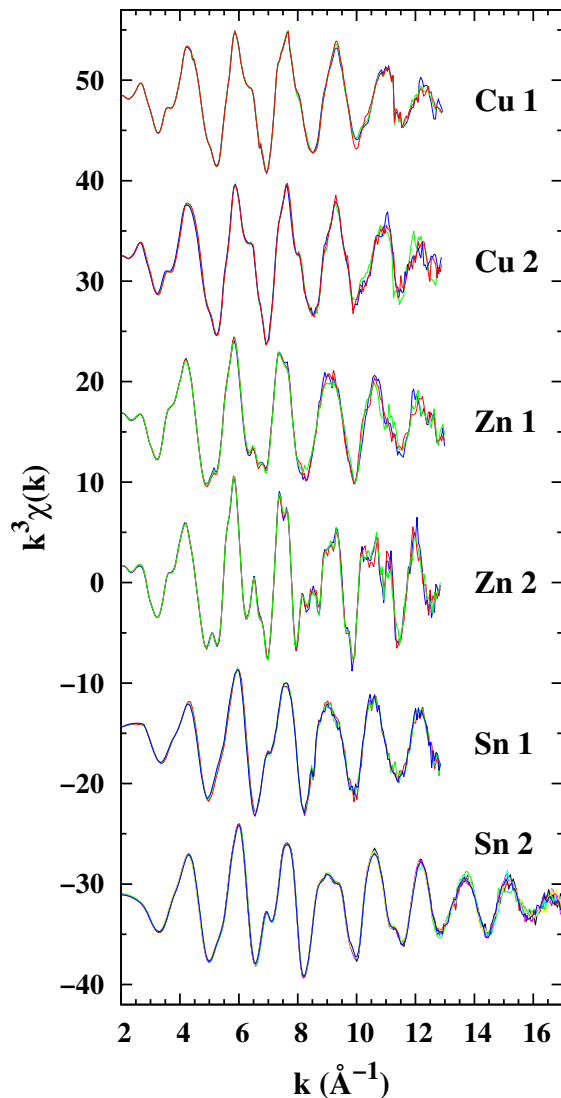
FIG. 2: k-space data ($k^3\chi(k)$) for the Cu K, Zn K, and Sn K edges of two CZTS samples at $T = 50$ K (#1) and 8 K (# 2). Three traces are plotted for each edge (seven traces for Sn 2) to show the reproducibility of the data. The largest difference between the samples is observed for the Zn K edge.

sion data and extracting the EXAFS oscillations, $\chi(E)$, with a spline fit of the post-edge background. This function was converted to k-space using the relation $k = \sqrt{(2m(E - E_0))/\hbar^2}$, where E_0 is experimentally determined as the energy at the half height of the edge step. The k-space EXAFS data for each metal K edge are shown in Fig. 2, and are highly reproducible with little variation between scans. Note that the Sn edge data of Sample #2 actually has seven data traces, which shows the high repeatability of the data. An average of these traces was used in the following data analysis and fits.

The k-space data were fast Fourier transformed (FFT)

into r-space using an FT range of 3.5–11.5 Å^{-1} (the FT window was Gaussian rounded by 0.3 Å^{-1}), as shown in Fig. 3 for a k^3 weighting - FFT($k^3\chi(k)$). Peaks in r-space correspond to different shells of neighbors, but the peak positions are always shifted to lower r compared to the actual pair distance - in this case by ~0.4 Å for S neighbors. For well ordered material, peaks exist well beyond 6-7 Å; generally the larger the amplitudes of the further neighbor peaks are, the more ordered the compound is. For all three edges, but particularly for Zn, Sample #2 has more well-defined peaks at high r, which means it is more ordered than Sample #1.

B. Composition

The composition results for the two samples are shown in Table I. These were determined from the absorption step height for each edge, measured at the same point on the same sample in a difference set of scans. Note that for such measurements, the sample needs to be thin enough so that the step height for the lowest energy edge was not too large (< 1); otherwise pinhole effects[28,29] distort the edge and make the observed step height too small. The step heights were converted to concentration ratios using the McMaster tables,[30] following the approach we have used successfully in the past.[20,21] Sample #1 contains too much Sn in the sample, with some Zn deficiency as well. For four S atoms (the EXAFS results presented later confirm the 4-fold S coordination of a kesterite structure for each metal atom), this yields a composition of $Cu_{1.89}Zn_{0.80}Sn_{1.31}S_4$, shown in Table I. In contrast, Sample #2 is instead Zn-rich with Sn close to stoichiometric, while still being Cu-poor. The resulting composition is $Cu_{1.75}Zn_{1.19}Sn_{1.06}S_4$. Samples #1 and #2 provide a means for studying how varying Sn concentrations influences the distribution of the metal atoms.

Ratios	#1	#2	Composition	#1	#2
Cu/Zn	2.37	1.47	Cu	1.89	1.75
Cu/Sn	1.45	1.64	Zn	0.80	1.19
Zn/Sn	0.61	1.12	Sn	1.31	1.06
Cu/(Zn+Sn)	0.90	0.77	S	(4)	(4)

TABLE I: Ratios of metal cations and relative composition of the CZTS samples, assuming four S atoms. These highlight the excess Sn and deficient Zn fractions in Sample #1, and the excess Zn and deficient Cu in Sample #2.

The off-stoichiometric composition raises several questions - are other phases present and if not, how are the Cu, Zn, and Sn arranged in the kesterite structure? From the later EXAFS analysis we will argue that possible phases such as ZnS or Cu_2SnS_4 etc. are at most a few percent and therefore concentrate here on the kesterite structure including possible antisite defects. Specifically for the twelve second neighbor metal atoms, what is the
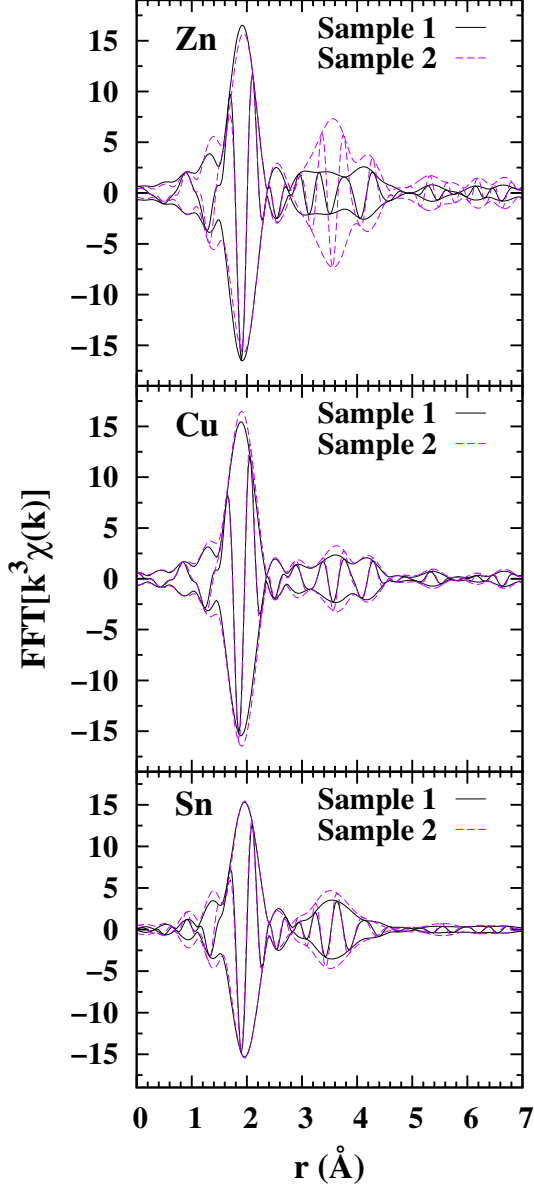
is that no site has second neighbors of the same site – e.g. the metal neighbors on S1 have four atoms each on sites S2, S3, and S4. Thus if a type of atom is only on one site (as is the case for Sn in stoichiometric CZTS), there will be no Sn neighbors about any Sn atom. If the fractional occupancy on each site is known one can easily calculate the number of Cu/Zn and Sn neighbors about Cu, Zn, or Sn. Based on earlier work that showed that CuS and ZnS do not mix[5], the occupation of each site was set by the following assumptions: 1. No exchange of Cu and Zn between their sites; and 2. Excess Sn can go onto either Cu or Zn sites. For sample # 1, excess Sn was placed on both the Cu and Zn site to give the following distribution on the four sites: $[Cu][Cu_{0.89}Sn_{.11}][Zn_{0.8}Sn_{0.2}][Sn]$. Sample #2 has excess Zn; in this case the excess Zn was placed on the Sn site and some Sn was shifted to a Cu site to give: $[Cu][Cu_{.75}Sn_{.25}][Zn][Sn_{0.81}Zn_{0.19}]$. [Note that if the excess Zn were placed on Cu sites, then there would be very few Sn neighbors about Sn - in strong disagreement with the results discussed below.] From these distributions the expected number of neighbors about Cu, Zn and Sn are calculated and tabulated in Table II.

	Sample #1		Sample #2	
Metal edge	M-Cu/Zn	M-Sn	M-Cu/Zn	M-Sn
Cu	7.0	5.0	8.2	3.8
Zn	7.6	4.4	8.3	3.7
Sn	10.0	2.0	10.5	1.5

TABLE II: Number of Cu/Zn and Sn neighbors about Cu, Zn, and Sn for samples #1 an #2, based on the distributions on each site described in the text: $[Cu][Cu_{0.89}Sn_{.11}][Zn_{0.8}Sn_{0.2}][Sn]$ and $[Cu][Cu_{.75}Sn_{.25}][Zn][Sn_{0.81}Zn_{0.19}]$.

C. Local Structure

The r-space data for the Cu, Zn, and Sn K edges look very similar in shape as shown in Fig. 3. The large peak near 1.9 Å corresponds to the four S atoms in the first shell of neighbors around each metal atom (actual distances from diffraction $\sim$2.33 – 2.4 Å). The position of this peak is nearly the same for each edge, suggesting comparable metal-S bond lengths. This is expected in CZTS but not for individual sulfides such as CuS and Cu_2S (shorter Cu-S bonds) or SnS and SnS_2 (longer Sn-S bonds). The second shell peak, near 3.5 Å (actual distance $\sim$3.8 Å), consists of 12 metal neighbors of Cu, Zn, or Sn for bulk material, but might be somewhat less for very small nanoparticles, depending on size; e.g. for $\sim$ 3 nm ZnS particles there are about 9-10 Zn second neighbors[24]. Note the peak positions are nearly the same for all edges as also observed by Espinosa-Faller et $al.$.[16] In contrast, Bacewicz et $al.$[14], find the Metal-Metal peaks at a longer distance, while Siah et $al.$[12] find the first Metal-S peaks at distances with even greater deviations from diffraction results, with negative shifts of 0.07-0.08

FIG. 3: EXAFS r-space data for the Zn, Cu, and Sn K edges of Samples #1 and #2. The strong similarities in shape indicate all the elements are in a similar environment. The largest peak near 1.9 Å is the first S neighbor. Here and in following r-space plots the fast oscillation is the real part, R, of the FFT; the amplitude function is $\pm \sqrt{R^2 + I^2}$ where I is the imaginary part (not plotted) of the FFT. FT window: 3.5–11.5 Å^{-1}, Gaussian broadened by 0.3 Å^{-1}.

atomic distribution about a given element? Because Cu and Zn are neighbors on the periodic table, such neighbors cannot be discriminated and only the numbers of Cu/Zn and Sn are considered. The kesterite structure has four distinct metal sites, M1-M4, occupied by Cu1, Cu2, Zn and Sn. An interesting feature of this structure
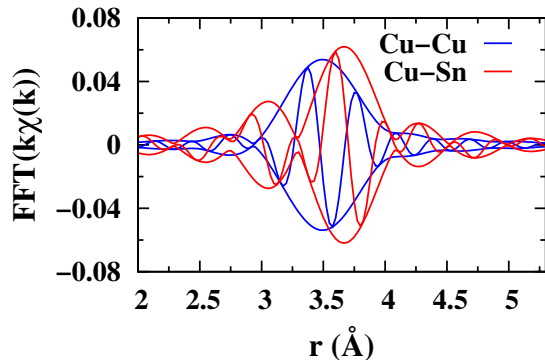
FIG. 4: A comparison of the theoretical r-space functions for Cu-Cu and Cu-Sn second neighbor peaks (these functions correspond to one neighbor at the same distance and are not broadened). Note that the real part of the Fourier Transform (fast oscillating function) for Cu-Cu is nearly 180° out of phase with that for Cu-Sn; consequently, a sum of these functions will be significantly reduced, and the peak position may be shifted.

Å for Zn-S and positive shifts of 0.06-0.07 Å for Sn-S, though they only report Δr without stating the starting pair distance.

Another unusual feature of our data comes from a comparison of the Cu and Zn K edge data; because Cu and Zn are neighbors in the periodic table, the simulated EXAFS using FEFF8.5[31] are essentially identical. Experimentally however, the second neighbor peak in the Zn edge data is much larger than for the Cu edge data, particularly for sample #2. A similar result was shown in r-space plots by Espinosa-Faller $et\ al.$;[16] the similarity might be related to the fact that both their study and ours use nanoparticle samples; however as discussed below it is more likely the distribution of atoms on the various sites.

Theoretical functions for each atom pair were generated using FEFF8[31]. Note that the second neighbor Cu and Zn backscatterers are nearly indistinguishable – i.e. the Metal-Cu and Metal-Zn functions are nearly the same. Consequently, in fits, a Cu second neighbor pair function was used to represent both the Cu and the Zn second neighbors. In contrast, the complex parts of the theoretical function for the Sn second neighbor are out of phase with that for the Cu and Zn functions, as shown explicitly in Fig. 4. Thus a sum of Cu-Cu and Cu-Sn functions will interfere destructively leading to a low amplitude. This makes it difficult to analyze the second neighbor data without detailed fits.

The EXAFS data also show that both samples have a significant amount of disorder for the second neighbors and beyond. Although the first peak has a large amplitude, the second peak is small compared to theoretical EXAFS functions for undistorted CZTS or EXAFS data for pure ZnS.[5,24]

IV. DATA ANALYSIS

A. General Fitting & Constraints

The kesterite structure, shown in Fig. 1, has a lower formation energy than the stannite structure, and thus is the more stable structure.[32] A comparison of kesterite and stannite bond lengths, as measured by diffraction,[33] is shown in Table III. The bond lengths of the two structures are within ∼0.01 Å of each other, which is indistinguishable to EXAFS. Although all the Metal-Metal distances are the same within ± 0.01Å for the kesterite structure, the first Sn-S bond is significantly longer (0.08 Å) than either Zn-S or Cu-S, while the second Sn-S is slightly shorter (-0.03 Å) than the corresponding second Cu-S or Zn-S distances. This indicates some M-S-M bond bending within the kesterite structure.

Using the space group parameters for kesterite Cu_2ZnSnS_4 ($I\bar{4}$ space group, a = 5.427 Å and c = 10.848 Å)[33], theoretical EXAFS functions were calculated for each pair of atoms (Metal-S, Metal-Cu/Zn, Metal-Sn, and the longer Metal-S) using the program FEFF8.5[31]. The first shell of neighbors around the metal atoms in Cu_2ZnSnS_4 contains four S atoms at distances of 2.3-2.4 Å (see Fig. 1 and Table III). The second shell of neighbors about the metal atoms contains the first metal neighbors at a distance of ∼3.8 Å; the longer metal-S bond (∼4.5 Å) is included to improve the fit results. These bond lengths, as measured by diffraction,[33] are shown in Table III. The inclusion of a weak multiscattering peak slightly improved the fits above 4.5 Å, but had no significant effect in the 3-4 Å range. Including this small contribution, there were 5 peaks in the fits.

The data were then fit in r-space to a sum of these EXAFS functions; in principle, there are three parameters per atom-pair - amplitude, position (r) and the width σ, of the pair distribution function. σ^2 models thermal and static disorder which lead to a reduction in peak amplitudes. Constraints must also be included as otherwise there would be too many free parameters, as discussed by Stern[34].

Since the amplitude for a given pair is given by $NS_\circ^2$, where $S_\circ^2$ is an amplitude reduction factor from multiscattering, $S_\circ^2$ needs to be measured separately. We determined it using the individual sulfides (CuS, ZnS, SnS_2) and used those values for each metal cation (0.85 for Cu, 0.95 for Zn, and 1.00 for Sn).

The Cu K, Zn K, and Sn K edge data for Cu_2ZnSnS_4 (see Fig. 3) were fit using a k-range of 3.5–11.5 Å^{-1} for Cu and Zn, and 3.5–12.5 and 3.5–15.5 Å^{-1} for Sn samples #1 and #2, respectively. Fits were performed over r-ranges of 1.6–4.8 Å for all edges.

In the fits, the amplitudes and relative pair distances were initially constrained to be consistent with the known kesterite crystal structure as follows. The ratios of the amplitudes for each atom pair were constrained to the ratio of the coordination numbers N – i.e. 4 S first neighbors, 12 metal second neighbors, and 12 further S neigh-

bors. There are two Metal-Metal peaks: one for the Cu and Zn neighbors, and the other for the Sn neighbors. The number of each type of metal neighbor was started at the values given by diffraction (c.f. Table III), and then the ratio of (Cu/Zn):Sn neighbors was allowed to vary. This ratio of second neighbors is the only amplitude parameter that is varied. For the pair distances, we initially fixed the distance ratios to be that of the kesterite structure, but allowed an overall expansion or contraction – 7 parameters were varied (1 amplitude, 1 r, and 5 σ's); 11 degrees of freedom remain for Cu and Zn using Stern's criteria[34]. No significant change in the pair distances occurred when this constraint on distance ratios was released – 11 parameters were varied (5 r's, 5 σ's and the amplitude ratio for Sn/(Cu/Zn) for second neighbors); about 7 degrees of freedom remain for Cu and Zn, and 9 and 14 for the two samples at the Sn edge.

B.   Results

In the initial fits as described above, the pair distances agree with diffraction results for kesterite CZTS, as shown in Table III. The first neighbor distances are especially close, the difference is ≤ 0.01 Å for Zn–S and Sn–S. The largest variation, compared to bonds in the kesterite structure is observed for Cu–S, which contracted by ~ 0.02 Å. CuS and Cu_2S both have a significantly shorter average Cu-S bond length. The slightly shortened bond length in the nanoparticle samples is much closer to that of bulk CZTS. The consistency of the bond lengths affirms that the nanoparticles are within the desired zinc-blende-like structure. The largest deviation however is for the Sn-Sn peak in Sn K edge data; this pair is not present in the kesterite structure and requires some Sn on either a Cu or Zn site. Surprisingly this distance is significantly longer than expected - by ~ 0.1 Å.

The second shell of neighbors also has surprising results for these fits using five peaks. The fit to the Cu edge data did not have the theoretical 4 Sn neighbors and 8 Cu/Zn neighbors of the kesterite structure. Instead, the second neighbor peak appears to have significantly more Sn neighbors than expected, see Tables III and II. Because the Cu-Sn function is out of phase with that for Cu-Cu (See Fig. 4) there would be increased destructive interference with a larger Cu-Sn peak, which might partially explain the low amplitude for the second peak. However there is no distribution of Cu, Zn, and Sn on the four kesterite sites that yields significantly more Sn neighbors than Cu/Zn neighbors about Cu.

The excess number of Sn neighbors is also observed in the Zn fits for Sample #1; Table III shows there are $\sim$ 6.0 Sn neighbors, significantly more than for the kesterite structure and more than the calculated number in Table II - 4.4. In contrast the number of neighbors about Zn in the five peak fit for Sample # 2 agrees very well with Table II.
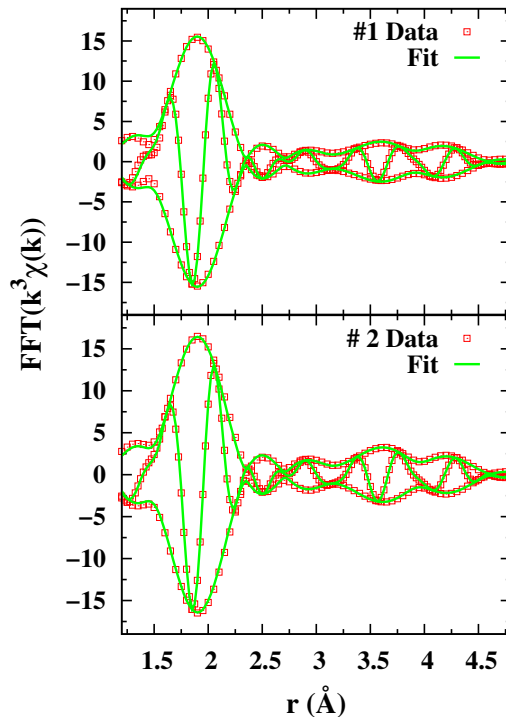

FIG. 5: Fit of the Cu K edge data using a sum of theoretical functions for kesterite Cu_2ZnSnS_4. The fit range was 1.6-4.8 Å for samples #1 and #2, and the FT range is 3.5-11.5 $Å^{-1}$. These fits used the two peak model for the Cu-Cu/Zn distribution as discussed in the text.

Finally, 5-peak fits were also performed on the Sn K edge data. The Sn-S bond length (~ 2.41 Å) is very close to that for the kesterite structure but significantly different from most other similar compounds; the Sn-Cu/Zn distance is also within ± 0.02 Å of the value for the kesterite structure. These results indicate that Sn is in a kesterite-like lattice. Based on this structure, Sn atoms should not have any Sn second neighbors; however, the fit of the Sn edge data shows there are ~ 2.9 Sn second neighbors present, even slightly higher than the estimates in Table II. Surprisingly, the number of Sn neighbors is roughly the same in both samples. To have Sn-Sn pairs, some antisite Sn must be on the Cu or Zn sites; the excess Sn stoichiometry for sample #1 explains much of the Sn-Sn amplitude. However sample #2 has nearly the stoichiometric amount of Sn (1.06) and if only 0.06 Sn were on either a Cu or Zn site, the resulting Sn-Sn peak would be very small. The significant Sn-Sn peak observed for this sample supports the assumptions made in Table II, namely that excess Zn does not go onto Cu sites, but onto Sn sites, with some Sn moving onto Cu sites. An important feature of the Sn fits is that the distance for the Sn-Sn peak is much longer than any other metal-metal pair distance.

Edge	Neighbor	N	Kesterite r_D (Å)	Stannite r_D (Å)	#1 r_E (Å)	σ^2 (Å²)	N	#2 r_E (Å)	σ^2 (Å²)	N
	S	4	2.328	2.319	2.307	0.00521	4	2.307	0.00476	4
Cu	(Cu/Zn)	8	3.837	3.828, 3.853	3.846	0.0091	4.0	3.857	0.00922	5.5
	Sn	4	3.837	3.828	3.839	0.0184	8.0	3.850	0.0159	6.5
	S2	12	4.517	4.520	4.502	0.0143	12	4.501	0.0132	12
	S	4	2.335	2.349	2.335	0.0054	4	2.337	0.0059	4
Zn	(Cu/Zn)	8	3.837	3.828	3.839	0.0137	6.0	3.838	0.0082	8.2
	Sn	4	3.836	3.853	3.839	0.0137	6.0	3.842	0.0085	3.8
	S2	12	4.501	4.510	4.470	0.0128	12	4.493	0.0099	12
	S	4	2.409	2.412	2.417	0.00372	4	2.407	0.00358	4
Sn	(Cu/Zn)	12	3.837	3.828, 3.853	3.820	0.0161	9.1	3.824	0.0123	9.1
	Sn	0	n/a	n/a	3.955	0.0113	2.9	3.921	0.0111	2.9
	S2	12	4.475	4.477	4.472	0.0155	12	4.464	0.0116	12

TABLE III: The first three columns show diffraction results for the bond lengths and number of neighbors (N) of kesterite and stannite Cu_2ZnSnS_4, generated from Hall et al.[33] using ATOMS.[35] The number of neighbors for these first four pairs is identical in the two structures. The final six columns show the Cu K, Zn K, and Sn K fit results for Cu_2ZnSnS_4 at 50 K for sample #1 and 8 K for # 2, assuming each metal pair can be modeled with a simple broadened Gaussian pair distribution and that the total number of metal second neighbors is 12. The EXAFS bond lengths (r_E) are in good agreement with diffraction results (r_D) at 300 K.[33] Although the second neighbor distances were initially constrained by the space group, no significant change in r occurred when this constraint was released. In these fits, except for the Zn K edge of sample #2, the number of Sn neighbors about each metal atom is too large compared to the kesterite structure and σ^2 for the M-M pairs is large. Errors for the first M-S peak are ± 0.01 Å for distance and ± 0.0004 Å² for σ^2; for the second M-S peak, ± 0.02 Å for the distance and ± 0.001 Å² for σ^2. Errors for Sn-M pairs are ± 0.02 Å for distance and 0.001 Å² for σ^2.

Further fits were performed to test whether the excess Sn could be reduced by adding extra Cu/Zn neighbors at a longer distance. The fits contained the two Metal-Metal peaks as before (Cu-Cu/Zn and Cu-Sn) with the addition of a second Cu-Cu/Zn bond. The extra peak did improve the fit slightly and reduced the number of Sn neighbors a little - but setting the number of Sn neighbors below 5 (see Table II) made the fit poor, particularly between 4 and 4.8 Å. Similar results were obtained for sample #1 at the Zn edge.

The possibility of a longer Cu/Zn bond was also tested for the Sn edge data. The fits contained two Cu/Zn peaks, with one peak initially at a larger distance from the core atom, Sn. The data do not fit this scenario; the long Cu/Zn peak has a huge σ^2 value of 0.159 Å^{-2}, and no longer contributes to the EXAFS plot.

It is surprising that the peak at 3.5 Å is so small in the Cu edge data and in the Zn edge data for sample # 1, as simulations are similar to but somewhat larger than the peak at 3.5 Å in the Zn edge data for sample # 2. In part, the sum of the Cu-Cu/Zn and Cu-Sn peaks near 3.5 Å is relatively small because these two functions are out of phase (See Fig. 4); but to get the very small amplitude observed requires a very large Cu-Sn peak to cancel the Cu-Cu/Zn peak. This is nonphysical; however the observed long Sn-Sn distance suggests an alternative possibility. This Sn-Sn distance only arises when there are antisite Sn defects on Cu or Zn sites. Since the first neighbor Sn-S bondlength is very close to that for the kesterite structure, 2.41-2.42 Å, but significantly longer (0.08 Å) than the Cu-S or Zn-S distances, antisite defects

will produce displacements of Cu or Zn atoms. Additionally, because the long Sn-Sn second neighbor distance is about 0.1 Å longer than Cu-Sn or Zn-Sn, there may also be significant changes in the Sn-S-Sn bond angle; increased and decreased bond angles will produce longer and shorter metal-metal pair distances.

One can model such distortions using a Cu-Cu/Zn (or Zn-Cu/Zn) pair distribution that is more complex than a simple Gaussian function. Conceptually, one could add peaks with shorter and longer distances (3 peaks total), but that would introduce 4-6 additional parameters, depending on constraints. Alternatively, one could use two Gaussians with quite different widths but the same r's to then only have 2 additional parameters (one extra σ and an amplitude ratio are needed).

Fits were carried out for these two more complex Cu-Cu/Zn (and Zn-Cu/Zn for sample #1) distributions; the 3-peak model fits best but was only slightly better than the 2-peak model with broad and narrow distribution widths. In addition, the ratio of neighbors for these two peaks was almost 1, and setting the amplitudes equal in further fits had very little effect on the quality of the fit. We therefore report the latter as it required only one additional parameter σ; those fits are shown in Fig. 5 for the Cu edge and in Fig. 6 for sample #1 at the Zn edge. The fit for sample #2 (Zn edge) in Fig. 6 used the 5-peak fit described earlier. Likewise the fits for the Sn edge in Fig. 7 also used the simpler 5-peak fit.

The results from the fits using two Cu-Cu/Zn (or Zn-Cu/Zn) peaks are given in Table IV. Although the number of Sn neighbors for the Cu edge data is slightly larger
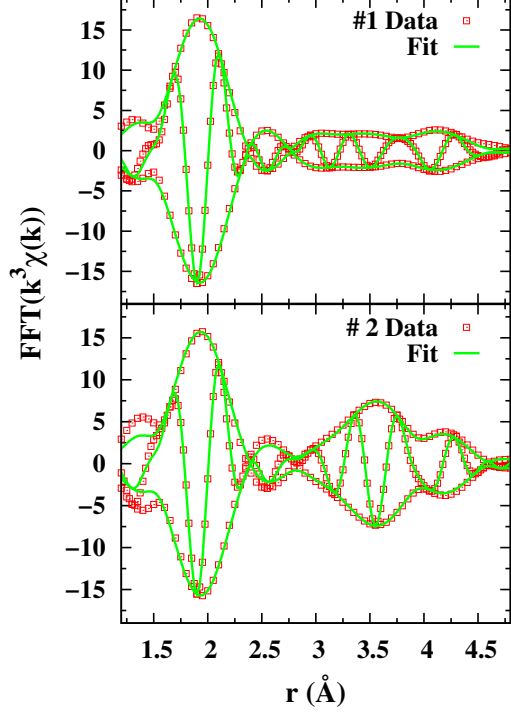
FIG. 6: Fit of the Zn K edge data for samples #1 and #2 using a sum of theoretical functions for kesterite Cu_2ZnSnS_4. The fit range is 1.6-4.8 Å for both samples, and the FT range is 3.5-11.5 Å^{-1}. For sample #1, the Zn-Cu/Zn peak is modeled using two peaks, one narrow and the other broad.

FIG. 7: Fit of the Sn K edge data for samples #1 and #2 using a sum of theoretical functions for kesterite Cu_2ZnSnS_4. The fit range is 1.6-4.8 Å for both samples, and the FT range is 3.5-12.5 Å^{-1} and 3.5-15.5 Å^{-1} for samples #1 and #2, respectively.

than the estimates in Table II, these are reasonable values considering the fact that the disorder is likely more complex. This, together with the 180° phase shift between Cu-Cu/Zn and Cu-Sn, provides a simple explanation as to why the net peak at 3.5 Å is so small.

For sample # 2 there is excess Zn and some Zn was assumed to move to the Sn sites – see Table II. However there is then no Sn on the Zn sites. Consequently the distortions about Zn may be smaller. In fact the amplitude for Zn-Zn/Cu is more than a factor of two larger (at 3.6 Å) compared to sample # 1. This unusual difference is now easily explained by much less disorder about Zn atoms, because there are no antisite Sn atoms on Zn sites.

The important point in using the 2-peak (or 3-peak) model is that it allows for a broader distribution of pair distances, with some distances longer or shorter by roughly the lengthening of the Sn-Sn peak; the Sn-Sn peak can only occur when Sn antisite atoms occupy Cu or Zn sites.
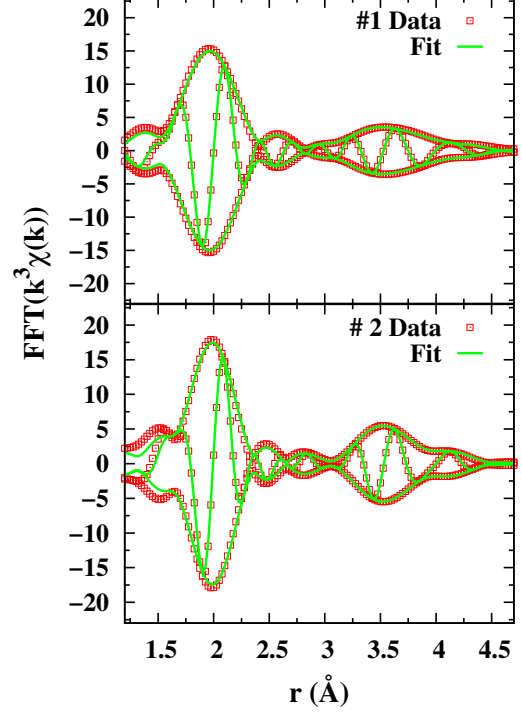
V. DISCUSSION

All three edges (Zn, Cu, and Sn K) indicate an excess of Sn second neighbors. This is consistent with Sn substituting on Cu or Zn sites to form antisite defects in the kesterite structure. Since Cu and Zn are indistinguishable, as mentioned before, the presence of Sn second neighbors provides a strong constraint on the distribution of the metal atoms, particularly about the Sn site. The shortest Sn-Sn distance is significantly longer than other metal-metal distances, which in turn suggests that the Sn antisite defects may introduce significant disorder about Cu and Zn, and lead to split Cu-Cu/Zn or Zn-Zn/Cu peaks as discussed in the 2-peak model above (See Table IV). However, can one exclude the possibility that other impurity phases lead to the number of neighbors and distances observed in Table III instead of using the 2-peak model?

First, the M-S bondlengths are all close to that expected for the kesterite structure, which excludes significant fractions of CuS or Cu_2S (Cu-S bonds too short) and SnS or SnS_2 (Sn-S bonds too long) as noted earlier. The M-S peaks are also quite sharp with values of $\sigma \sim 0.07$ Å ($\sigma^2 \sim 0.005$ Å^2). Since part of this width

Edge	Neighbor	N_K	#1			#2		
			r_E (Å)	σ^2 (Å²)	N_E	r_E (Å)	σ^2 (Å²)	N_E
Cu	(Cu/Zn)-a	8	3.86(2)	0.0024(5)	3.4(4)	3.85(2)	0.0025(5)	3.4(4)
	(Cu/Zn)-b		3.86(2)	0.034(2)	3.4(4)	3.85(2)	0.017(1)	3.4(4)
	Sn	4	3.81(2)	0.0085(5)	5.2(4)	3.82(2)	0.0091(5)	5.2(4)
Zn	(Cu/Zn)-a	8	3.85(2)	0.0072(5)	3.3(4)	3.84(2)	0.0082(5)	8.2(4)
	(Cu/Zn)-b		3.85(2)	0.014(1)	3.3(4)			
	Sn	4	3.85(2)	0.0126(5)	5.4(5)	3.84(2)	0.0085(5)	3.8(4)

TABLE IV: Results for the fits using two Cu-Cu/Zn or Zn-Cu/Zn peaks for Cu and Zn edges. N_K gives the number of neighbors in the kesterite structure. For the Zn edge data of sample #2, two Zn-Cu/Zn peaks were not needed; the values with a single peak for Zn-Cu/Zn are included for comparison. Errors are estimated from a range of fits using different starting assumptions; distances have little variation but there are much larger variations for N and σ^2.

arises from zero-point-motion, there is very little variation in the M-S bondlengths. This is consistent with the kesterite structure, for which there is one M-S bond length for a given M atom, although bond lengths for different M atoms vary - from 2.31 Å for Cu-S to 2.41 Å for Sn-S. These sharp distributions discriminate against many other compounds such as $Cu_4Sn_4S_{16}$ and Cu_4SnS_4 which have a broad distribution of Cu-S distances; significant fractions of such compounds would lead to a small Cu-S peak. For compounds such as Cu_2SnS_3 there are very nearly twice as many Cu neighbors as Sn neighbors about Cu (as a result of Cu and Sn sharing two sites in the structure), while for the perfect kesterite structure there are exactly twice as many Cu/Zn neighbors as Sn around Cu; thus a significant fraction of this compound could not lead to a smaller number of Cu-Cu/Zn pairs than Cu-Sn pairs. In addition, the Sn-S bond in Cu_2SnS_3 (2.36 Å) is shorter than the Sn-S distance observed in CZTS (2.41 Å) while the Sn-Sn distance in Cu_2SnS_3 (3.83 Å) is much shorter that the Sn-Sn distance observed for CZTS (3.92-3.95 Å). Thus a significant fraction of ZnS plus Cu_2SnS_3 would not have the distances and amplitudes observed.

$Cu_2Sn_4S_9$, on the other hand, has no Cu or Sn neighbors at distances below 4.3 Å for the Cu site, but six Sn neighbors (and no Cu below 4.3 Å) about the Sn site. These properties are not consistent with the observed distances for Cu-Cu or Cu-Sn near 3.8 Å, or the large number of Cu neighbors about Sn (Table III). We conclude that the best description of the data is a kesterite structure with antisite defects present to accommodate the off-stoichiometry. When antisite Sn defects are present they introduce larger distortions, and broadened pair distribution functions (2-peak model) for Cu-Cu/Zn or Zn-Cu/Zn pairs are needed. Small fractions of other phases can not be entirely excluded but are estimated to be at most 5%.

A few other papers use EXAFS to examine CZTS materials, with some differing results. Hartman et al.[13] detect the presence of ZnS in CZTS thin films by looking at the Zn edge of the data. Their results use EXAFS only for the Zn edge and would be strengthened by data for the other edges. Siah et al.[12] look at the metal and S K edges in their EXAFS analysis of the effect of excess Zn, presumably at 300K. In contrast to Hartman et al.,[13]

their study finds that excess Zn is actually incorporated into the CZTS structure via antisite defects and is assumed to be uniformly distributed between Cu and Sn sites, instead of forming ZnS. This partially agrees with our results, which suggest similar antisite defects, but our results for a sample with significant excess Zn suggest that the excess goes more onto Sn sites. This agrees with earlier work that shows that Cu_2S and ZnS are nearly immiscible[5]. No analysis of the second neighbor (M-M) peaks is provided in this paper, and the M-S bond lengths have much larger deviations from the kesterite structure (up to 0.07 Å) than in the results reported here.

A third paper reporting EXAFS of CZTS (Bacewicz et al.[14]) examines all three metal cation edges in powder samples of CZTS. Their second neighbor distances agree quite well with our results, although their powders are close to stoichiometric. They propose that Sn is primarily on its native site, but admit some may be on Cu and Zn defect sites.

Data et al.[36] also carried out EXAFS measurements on nanoparticles, presumably at 300K, and find considerable disorder for the further neighbor shells. Their metal-S distances agree with our results within 0.01 Å, but they provide no analysis for the further neighbors. Espiosa-Faller et al.[16] also agree with our results for the first neighbor metal-S pairs - to within 0.01 Å. However, the second neighbor results of our study cannot be directly compared with Espinosa-Faller et al.[16] because their analysis describes a different number of second neighbors than the kesterite structure. The authors describe the theoretical crystal structure for each of the metal cations as only having 8 metal second neighbors instead of the 12 given by the structure.[14,33] In Table 2 of their paper,[16] Cu is listed as only having 4 Cu/Zn neighbors, when it should have 8. Espinosa-Faller et al. also describe Zn as having 4 Zn second neighbors, even though the kesterite structure contains no Zn second neighbors and 8 Cu second neighbors. Similarly, Sn is described by them to have 8 Cu/Zn neighbors instead of the expected 12. Finally, their table lists 8 neighbors for the second Metal-S peak rather than 12 neighbors. The differences in number of neighbors directly influences the σ^2 values, so these disagreements obstruct comparisons.

Even with the discrepancies for the further neighbors, we agree with the Espinosa-Faller result of site-antisite cation exchange within the crystal structure. The antisite substitution is further supported in that we see no evidence for any interstitial sites in our EXAFS results. Although Espinosa-Faller *et al.* included a few interstitial S sites in their fits of the EXAFS data, the other techniques they used found that interstitial sites played a negligible role. The addition of interstitial S is not required in our EXAFS analysis.

Very recently, Colina-Ruiz *et al.*[17] reported EXAFS at 80 K on highly non-stoichiometric CZTS films with Cu/Zn ratios as low as 1.03 (instead of $\sim$ 2) and Cu/(Zn+Sn) ratios down to 0.64. Thus some of their films are more non-stoichiometric than the materials considered here. Full details of their fits are not given but it appears they did not include the possibility of antisite defects in their fits of second neighbors and fixed the amplitudes to that for the kesterite structure. In particular, for the Sn K edge they did not include any Sn-Sn peak and assumed the Sn-Cu/Zn peak had only 8 neighbors. Thus comparisons with their work for the second neighbor peaks are not straightforward as they provide no information about possible antisite defects. However their M-S bond lengths do agree with ours for the samples closest to our compositions. Finally the bond lengths they tabulate for the kesterite structure do not agree well with the diffraction results of Hall *et al.*[33]; specifically they list the M-S bond lengths as all equal (2.35 Å), while Hall *et al.* give a short bond length for Cu-S (2.328 Å) and a long bond length for Sn-S (2.409 Å).

Nanoparticle films have been studied by Turnbull *et al.*[37] using several techniques including EXAFS. Their sample 1 has a similar composition to our sample #2, but none of the others are comparable to our sample #1 which has a high Sn and low Cu content. They report EXAFS results for the first two shells, S and metal neighbors. Unfortunately, the data they show for the Cu and Zn K edges have a very low amplitude for the second neighbors over the range 3-4.8 Å, in contrast to our data, or the results of Bacewicz *et al.*[14] and also Data *et al.*[36]. Thus it is not clear how they obtained detailed fits of the Cu-metal and Zn-metal peaks. Further, most of their reported Cu-metal and Zn-metal distances differ significantly from the kesterite structure; for example the Cu-Cu distances vary from 3.55 to 3.83 Å, while the Zn-Cu distances vary from 3.67 to 3.91 Å. Such large differences are not found in crystalline materials. In addition, the tabulated distances for the kesterite structure have errors, as there are no Zn-Zn or Sn-Sn second neighbors in a pure kesterite crystal. They also did not discuss the coordination numbers for the second neighbors which is crucial for probing the effects of non-stoichiometry. Consequently, it is not possible to compare with their results.

Lastly, several groups[12,17–19] have used the S K edge XANES to look at possible impurity phases in non-stoichiometric material. Colina-Ruiz *et al.*[17] used a linear combination of files for CZTS, ZnS, and SnS to fit their S

K edge XANES, while Just *et al.*[18] use a linear combination of only CZTS and ZnS scans. Siah *et al.*[12] used the height of the S pre-edge peak to estimate the amount of ZnS. It is not clear how unique these fits are as there are many more possible compounds that might be present (e.g. SnS_2, Cu_2SnS_3, $Cu_4Sn_4S_{16}$ and Cu_4SnS_4), all of which might contribute at the S K-edge. Note that most of the samples investigated by Just *et al.*[18] have Zn/Sn ratios much higher than our samples. Siah *et al.*[12] also focus mostly on Zn rich samples, while Colina-Ruiz *et al.*[17] have a broad range of stoichiometries. They report significant amounts of ZnS in some samples, but for samples with compositions similar to our materials, the amount of ZnS present is small.

VI. CONCLUSIONS

We have carried out a detailed EXAFS study of non-stoichiometric, Cu-deficient, nanoparticle CZTS to determine the structure about each metal atom and ascertain whether significant fractions of the sample might be in other crystalline phases. Cu-deficient material are of interest because several reports have suggested that such materials are better for devices[1,2,4,22]. From the perspective of EXAFS, these fairly large nanoparticles (7 nm) are close to bulk because the surface layer is only a small fraction of the nanoparticle.

The local structure for the two samples agrees well with the kesterite lattice, with antisite defects, particularly Sn on Cu or Zn sites, accommodating the non-stoichiometry. In particular the closest M-S bondlengths agree with this crystal structure within 0.01 Å for Zn and Sn, and 0.02 Å for Cu. Further the distributions of these bondlengths are very narrow ($\sigma \sim 0.07$ Å); together these results indicates that most of the metal atoms are in the kesterite structure and not in some other phases that have different M-S bondlengths such as CuS, Cu_2S, SnS and SnS_2.

In the Sn edge data there are a significant number of second neighbor Sn atoms observed; since for stoichiometric CZTS there would be no Sn neighbors, this indicates Sn antisite defects are present on Cu or Zn sites. Surprisingly the Sn-Sn pairs have a significantly larger pair distance than other M-M pairs, by $\sim$ 0.1 Å; this means there are important local distortions around the antisite Sn defects. This will lead to broadened distributions for the metal-metal second neighbor pairs. In the initial fits we modeled each pair using a single broadened peak (e.g. Cu-Cu/Zn and Cu-Sn for the Cu edge) but found non-physical results in that there appeared to be more Cu-Sn pairs than Cu-Cu/Zn pairs about Cu. However broadening the Cu-M further using a 2-peak distribution with different widths (or a split peak distribution) models the environment about Cu in both samples and about Zn in sample # 1, very well. The distortions about Sn are slightly smaller and reasonably well described by just a broadened Sn-Cu/Zn peak.

The results are also consistent with the assumptions

used for Table II, namely that most of the excess Zn in sample #2 does not go onto Cu sites but rather onto Sn sites, forcing some Sn to move to Cu sites, thereby explaining the Sn-Sn peak observed in this sample. This is consistent with earlier work that shows CuS (Cu$_2$S) and ZnS are not compatible;[5,25,38] note this does not exclude low concentrations of antisite defects Cu$_{Zn}$ or Zn$_{Cu}$, which are often present.[6]

These results will be important for theorists trying to model off-stoichiometric material for optimization of properties. Sn antisite defects appear to form readily on Cu or Zn sites in Cu poor samples and our results are consistent with excess Zn preferring Sn site occupation over Cu site occupation.

More generally, EXAFS is shown to be a good tool for studying the local structure of CZTS, which is likely more complicated than stoichiometry suggests. Understanding these structural variations may be a key step to improving solar energy conversion efficiencies.

Acknowledgments

[*] Correspondence:`bridges@ucsc.edu`

[1] W. Wang, M. T. Winkler, O. Gunawan, T. K. Todorov, Y. Zhu, and D. B. Mitzi, Device Characteristics of CZTSSs Thin-Film Solar Cells with 12.6% Efficiency, Ad. Energy Mater. **4**, 1301465 (2014).

[2] Q. J. Guo, G. M. Ford, W. C. Yang, B. C. Walker, E. A. Stach, H. W. Hillhouse, and R. Agrawal, Fabrication of 7.2% Efficient CZTSSe Solar Cells Using CZTS Nanocrystals, J. Am. Chem. Soc. **132**, 17384–17386 (2010).

[3] H. Katagiri, K. Jimbo, W. S. Maw, K. Oishi, M. Yamazaki, H. Araki, and A. Takeuchi, Development of CZTS-based thin film solar cells, Thin Solid Films **517**, 2455–2460 (2009), doi:10.1016/j.tsf.2008.11.002.

[4] S. Siebentritt and S. Schorr, Kesterites: a challenging material for solar cells, Progress in Photovoltaics: Research and Applications **20**, 512–519 (2012), doi:10.1002/pip.2156.

[5] A. Short, L. Jewell, A. Bielecki, T. Keiber, F. Bridges, S. A. Carter, and G. Alers, Structure in multilayer films of zinc sulfide and copper sulfide via atomic layer deposition, J. Vac. Sci. and Tech. A **32**, 01A125 (2014).

[6] S. Chen, J.-H. Yang, X. G. Gong, A. Walsh, and S.-H. Wei, Intrinsic point defects and complexes in the quaternary kesterite semiconductor Cu$_2$ZnSnS$_4$, Phys. Rev. B **81**, 245204 (2010).

[7] C. Malerba, F. Biccari, C. L. Azanza Ricardo, M. Valentini, R. Chierchia, M. Müller, A. Santoni, E. Esposito, P. Mangiapane, P. Scardi, and A. Mittiga, CZTS stoichiometry effects on the band gap energy, J. Alloys Compds. **582**, 582–534 (2014), doi:10.1016/j.jallcom.2013.07.199.

[8] D. B. Mitzi, O. Gunawan, T. K. Todorov, and D. A. R. Barkhouse, Prospects and performance limitations for CuZnSnSSe photovoltaic technology, Phil. Trans. R. Soc. A **371**, 20110432 (2013), doi:10.1098/rsta.2011.0432.

[9] S. Schorr, The crystal structure of kesterite type compounds: A neutron and X-ray diffraction study, Solar Energy Materials & Solar Cells **995**, 1482–1488 (2011).

[10] S. Schorr, H.-J. Hoebler, and M. Tovar, A neutron diffraction study of the stannite-kesterite solid solution series, Eur. J. Mineral. **19**, 65–73 (2007).

[11] R. Nakamura, K. Tanaka, H. Uchiki, T. Washio, and H. Katagiri, Cu$_2$ZnSnS$_4$ thin film deposited by sputtering with Cu$_2$ZnSnS$_4$ compound target, Jap. J. Appl. Phys. **53**, 02BC10 (2014).

[12] S. C. Siah, R. Jaramillo, R. Chakraborty, P. T. Erslev, C.-J. Sun, T.-C. Weng, M. F. Toney, G. Teeter, and T. Buonassisi, X-Ray Absorption Spectroscopy Study of Structure and Stability of Disordered (Cu$_2$SnS$_3$)$_{1-x}$(ZnS)$_x$ Alloys, Photovoltaics, IEEE Journal of **5**, 372–377 (2015).

[13] K. Hartman, B. K. Newman, J. L. Johnson, H. Dui, P. A. Fernandes, V. Chawla, T. Bolin, B. M. Clemens, A. F. da Cunha, G. Teeter, M. A. Scarpulla, and T. Buonassissi, Detection of ZnS Phases in CZTS Thin-Films by EXAFS, Photovoltaic Specialists Conference (PVSC), 2011 37th IEEE 002506–002509 (2011).

[14] R. Bacewicz, J. Antonowicz, S. Posiadło, and S. Schorr, Local Structure in Cu$_2$ZnSnS$_4$ studied by the XAFS method, Solid State Commun. **177**, 54–56 (2014).

[15] W. Zalewski, R. Bacewicz, J. Antonowicz, A. Pietnoczka, T. Evstigneeva, and S. Schorr, XAFS study of kesterite, kuramite, and stannite type alloys, J. Alloys Compds. **492**, 35–38 (2010).

[16] F. Espinosa-Faller, D. R. Conradson, S. C. Riha, M. B. Martucci, S. J. Frederick, S. Vogel, A. L. Prieto, and S. D. Conradson, Neutron Diffraction and X-ray Absorption Fine Structure Evidence for Local Lattice Distortions and Aperiodic Antisite Substitution in Cu$_2$ZnSnS$_4$ Nanoparticles, J. Phys. Chem. **118**, 26292–26303 (2014).

[17] R. Colina-Ruiz, J. M. de Len, J. Lezama-Pacheco, F. Caballero-Briones, M. Acosta-Alejandro, and F. Espinosa-Faller, Local atomic structure and analysis of secondary phases in non-stoichiometric Cu2ZnSnS4 using X-ray absorption fine structure spectroscopy, J. Alloys Compds. (2017), doi: 10.1016/j.jallcom.2017.04.191.

[18] J. Just, D. Lutzenkirchen-Hecht, R. Frahm, S. Schorr, and T. Unold, Determination of secondary phases in kesterite Cu$_2$ZnSnS$_4$ thin films by x-ray absorption near edge structure analysis, Appl. Phys. Lett. **99**, 262105/1–3 (2011), doi= http://dx.doi.org/10.1063/1.3671994.

[19] J. Just, C. M. Sutter-Fella, D. Lutzenkirchen-Hecht, R. Frahm, S. Schorr, and T. Unold, Secondary phases and their influence on the composition of the kesterite phase in CZTS and CZTSe thin films, Phys. Chem. Chem. Phys. **18**, 15988–94 (2016), dOI: 10.1039/c6cp00178e.

[20] S. Jang, B. D. White, I. K. Lum, H. Kim, M. A. Tanatar,

W. E. Straszheim, R. Prozorov, T. Keiber, F. Bridges, L. Shu, R. E. Baumbach, M. Janoschek, and M. B. Maple, Resolution of the discrepancy between the variation of the physical properties of Ce(1-x)YbxCoIn5 single crystals and thin films with Yb composition, Phil. Mag. **94**, 4219–4231 (2014), http://dx.doi.org/10.1080/14786435.2014.976287.

[21] F. Bridges, C. MacKeen, and L. Kovács, No difference in local structure about a Zn dopant for congruent and stoichiometric $LiNbO_3$, Phys. Rev. B **94**, 014101 (2016).

[22] H. Katagiri and K. Jimbo, Development of rare metal-free CZTS-based thin film solar cells, Photovoltaic Specialists Conference (PVSC), 2011 37th IEEE 003516–003521 (2011).

[23] Q. J. Guo, H. W. Hillhouse, and R. Agrawal, Synthesis of Cu_2ZnSnS_4 Nanocrystal Ink and Its Use for Solar Cells, J. Am. Chem. Soc. **131**, 11672–11673 (2009).

[24] C. Corrado, Y. Jiang, F. Oba, M. Kozina, F. Bridges, and J. Z. Zhang, Synthesis, Structural, and Optical Properties of Stable ZnS:Cu,Cl Nanocrystals, J. Phys. Chem. A **113**, 3830 (2009).

[25] J. Stanley, Y. Jiang, F. Bridges, S. A. Carter, and L. Ruhlen, Degradation and rejuvenation studies of AC electroluminescent ZnS:Cu,Cl phosphors, J. Phys.: Condens. Matter **22**, 055301/1–15 (2010), doi:10.1088/0953-8984/22/5/055301.

[26] See http://lise.lbl.gov/RSXAP/.

[27] J. A. Victoreen, The calculation of X-ray mass absorption coefficients, J. Appl. Phys. **20**, 1141–1147 (1949).

[28] E. A. Stern and K. Kim, Thickness effect, Phys. Rev. B **23**, 3781 (1981).

[29] S. M. Heald, in X-Ray Absorption: Principles, Applications, Techniques of EXAFS, SEXAFS, XANES, edited by D. Koningsberger and R. Prins (John Wiley and Sons, New York, 1988), pp. 87–118.

[30] W. H. McMaster, Compilation of X-ray Cross Sections, UCRL-50174 Sec. II, Rev. 1 (Lawrence Radiation Laboratory, University of California, Berkeley, 1969).

[31] A. L. Ankudinov, B. Ravel, J. J. Rehr, and S. D. Conradson, Real Space Multiple Scattering Calculation of XANES, Phys. Rev. B **58**, 7565 (1998).

[32] M. Jiang and X. Yan, Cu_2ZnSnS_4 Thin Film Solar Cells: Present Status and Future Prospects, Solar Cells - Research and Application Perspectives **InTech**, 107–143 (2013).

[33] S. R. Hall, J. T. Szymanski, , and J. M. Stewart, Kesterite, $Cu_2(Zn,Fe)SnS_4$, and Stannite, $Cu_2(Zn,Fe)SnS_4$, Structurally Similar but Distinct Minerals, Can. Mineral. **16**, 131–137 (1978).

[34] E. A. Stern, Number of relevant independent points in X-ray-absorption fine-structure spectra, Phys. Rev. B **48**, 9825 (1993).

[35] B. Ravel, ATOMS: crystallography for the X-ray absorption spectroscopist, J. Synchrotron Rad. **8**, 314–316 (2001), doi:10.1107/S090904950001493X.

[36] P. Data, M. Bialoglowski, K. Lyzwa, R. Bacewicz, P. Dluzewski, M. Lapkowski, T. Gregorkiewicz, S. Podsiadlo, and A. P. Monkman, Kesterite Inorganic-Organic Heterojunction for Solution Processable Solar Cells, Electrochim. Acta **201**, 7885 (2016), http://dx.doi.org/10.1016/j.electacta.2016.03.132.

[37] M. J. Turnbull, D. Vaccarello, Y. M. Yiu, T.-K. Sham, and Z.Ding, Identifying barriers to charge-carriers in the bulk and surface regions of Cu_2ZnSnS_4 nanocrystal films by x-ray absorption fine structures (XAFSs), J. Chem. Phys, **145**, 204702 (2016), doi: 10.1063/1.4967863.

[38] E. Lendvay, Formation of Cu_xS and Zn secondary phases in ZnS single crystals, J.Cryst. Growth **59**, 384–390 (1982).